

Influence of the gravitational darkening effect on the spectrum of a hot, rapidly rotating neutron star

AGNIESZKA MAJCZYNA¹

—

JERZY MADEJ²

—

AGATA RÓŻAŃSKA³

—

MIROSLAW NALEŻYTY²

—

¹*National Centre for Nuclear Research, ul. Andrzeja Sołtana 7, 05-400 Otwock, Poland;*

²*Astronomical Observatory, University of Warsaw, Al. Ujazdowskie 4, 00-478 Warszawa, Poland;*

³*Nicolaus Copernicus Astronomical Centre, Polish Academy of Sciences, ul. Bartycka 18, 00-716 Warszawa, Poland;*

Submitted to ApJ

ABSTRACT

In this paper, we discuss the influence of the gravitational darkening effect on the emergent spectrum of a fast-rotating, flattened neutron star. Model atmosphere codes always calculate spectra of emergent intensities and fluxes emitted from the unit surface on the star in plane-parallel geometry. Here we took a step beyond that and calculated a small sample grid of theoretical spectra integrated over the distorted surface of a sample rotating neutron star seen by a distant observer at various inclination angles. We assumed parameters like two dimensionless angular velocities $\bar{\Omega}^2 = 0.30$ and 0.60 , the effective temperature of a nonrotating star $T_{\text{eff}} = 2.20 \times 10^7$ K, the logarithm of the surface gravity of a spherical star $\log(g) = 14.40$ (cgs), and inclination angles from $i = 0^\circ$ to $i = 90^\circ$ with step $\Delta i = 10^\circ$. We assumed that the atmosphere consists of a mixture of hydrogen and helium with $M_{\text{H}} = 0.70$ and $M_{\text{He}} = 0.30$. At each point on the neutron star surface, we calculated true intensities for local values of parameters (T_{eff} and $\log(g)$), and these monochromatic intensities are next integrated over the whole surface to obtain the emergent spectrum. In this paper, we compute for

the first time theoretical spectra of the fast-rotating neutron star. Our work clearly shows that the gravitational darkening effect strongly influences the spectrum and should be included in realistic models of the atmospheres of rotating neutron stars.

Keywords: radiative transfer – gravitational darkening effect – stars: neutron

1. INTRODUCTION

A star distorted by either the centrifugal force caused by rotation or by tidal forces from a secondary star in a close binary system radiates away radiative energy in a nonsymmetric way and exhibits variations of the radiation power over its surface. Consequently, the effective temperature on the stellar surface is not uniform. The effect was recognized by Hugo von Zeipel in 1924 (von Zeipel 1924). He investigated the radiative stellar interior in hydrostatic equilibrium. The main conclusion of his work was that the locally emergent bolometric flux of the radiation of a distorted star is proportional to the local gravity. Assuming of Stefan-Boltzmann law, it could be written as $T_{\text{eff}} \sim g^{1/4}$, known as the *von Zeipel law*. The results of von Zeipel are valid only for stars with fully radiative envelopes and hydrostatic equilibrium. This law must be written in the more general form as $T_{\text{eff}} \propto g_{\text{eff}}^{\beta}$, where β is the *gravitational darkening exponent* (GDE). If the envelope of the star is not fully radiative, the gravitational darkening exponent differs from 1/4.

The literature on the theory of stellar atmospheres involves the following terms: the gravitational darkening and the limb darkening. We direct the attention of the reader to the basic difference between these two terms. Limb darkening is an optical effect seen both in spherical and distorted stars where the central part of the star's disk is brighter than the star's limb. This effect denotes that the specific intensity of the radiation emitted at some point on the surface is the largest in the vertical direction and decreases in directions approaching the horizontal plane for a single value of the effective temperature at this point. Gravitational darkening denotes that the value of the effective temperature (total luminosity) varies over the surface of the distorted star. The distortion of the star can be caused either by centrifugal forces due to rotation or by tidal interactions between two stars in a close binary system.

Gravitational darkening effects were studied for different aspects and for different types of objects (see e.g. Djurašević et al. 2003, 2006; Domiciano de Souza et al. 2014). Theoretical models of gravitational darkening for different types of objects were also developed. Lucy (1967) investigated a fully convective envelope and found that $\beta \sim 0.08$. This is a very weak dependence of the effective temperature on the effective gravity. The results of Lucy (1967) research were confirmed by Webbink (1976), who used a simple opacity law. The author presented an approximation, which under the assumption of constant entropy of the envelope, gave results consistent with those obtained by Lucy (1967). Note, that all these above results were obtained under

assumptions of rigid and small rate of rotation. In the case of neutron stars, the latter assumption is not strictly valid.

Recently Claret (2015) investigated gravitational darkening for neutron stars with various rotational models assumed. The author assumed a spherical shape of the neutron star and explored the dependence of β on the temperature of the star. There is a weak dependence of the gravitational darkening exponent on the temperature below 6×10^7 K in all assumed models of the rotation. In the above paper, the author was concerned about the calculation of the gravitational darkening exponent and its dependence on the rotation law. The author did not calculate any model spectra of a rotating star, either normal or neutron star.

The equilibrium configurations of a slowly rotating neutron star for different central densities ρ_c and circular angular velocities Ω were investigated by Belvedere et al. (2014). The most interesting result of this paper was presented in their Figure 16, where the authors have shown the dependence of the eccentricity on the frequency of the neutron star rotation. What is important, for frequency typical for neutron stars in X-ray bursters the eccentricity is of the order of 0.6, which means that the ratio of the polar radius to the equatorial radius $R_p/R_{eq} \sim 0.8$. We expect that such flattening should give rise to visible changes in the emerging spectrum.

The effective surface acceleration of the rotating neutron star was calculated by AlGendy & Morsink (2014) by using useful approximate formulae. On the surface of an oblate star, the effective gravity acceleration is decreased by the centrifugal force at the equator and increased by the centrifugal flattening of the star. The authors have shown useful formulae on the effective gravity for the approximation of fast and slow rotation. These formulae weakly depend on the chosen equation of state of the neutron star matter. In the slow rotation approximation, the effective gravity depends only on the compactness ratio M/R_{eq} , the dimensionless square of the angular velocity $\Omega^2 R_{eq}^3/GM$, and the latitude on the surface of the star. For spin frequency ~ 600 Hz difference of the effective gravity between the pole and equator is about 20%. This effect is important not only for the spectrum calculation but, also for it influence on the Eddington luminosity of a neutron star. AlGendy & Morsink (2014) have shown that for the assumed $\bar{\Omega}^2 = 0.1$, the expected difference between the Eddington luminosity at the pole and at the equator is about 10%. This is crucial because X-ray bursts at the Eddington limits (PRE - photospheric radius expansion bursts) are used as the standard candles (Galloway et al. 2008).

Suleimanov et al. (2020) investigated the spectra of slowly rotating neutron stars for a few models of the emission, from the simplest blackbody to their theoretical model atmospheres. Using their models, the authors calculated the dilution factor w and the spectral hardening factor f_c to obtain local specific intensities, which are next integrated over the surface of the star. Different rotational frequencies and inclination angles were investigated. The shape of the star and the local gravity are

calculated under the approximation of slow rotation. General relativistic effects were also included.

We note here that [Jaroszynski \(1986\)](#) modeled the external gravitational field and surface shape of neutron stars rotating with the single angular velocity $\Omega = 0.27GM/R^3$. [Jaroszynski \(1986\)](#) investigated the influence of the rotation on the observed luminosity and spectrum of the rotating neutron star. For the assumed angular velocity, eccentricity, and other basic parameters of the star, spectra have been calculated. Even if the blackbody model was used for the spectrum, the light bending was included. The ray-tracing procedure was included by the author. The main conclusion of [Jaroszynski \(1986\)](#) was that a two-temperature blackbody shape is needed to fully describe the spectrum of the rotating star. The author also showed that a small, 10%, changing eccentricity cannot be seen in the emerging spectrum.

In this paper, we show how fast rotation and therefore the gravitational darkening effect influences the shape of the spectrum of the oblate neutron star. Emergent spectra of the rotating neutron star seen by a distant observer are calculated by the ATM24 code, which solves the full radiative transfer including Compton scattering (see e.g. [Majczyna et al. 2005](#); [Madej et al. 2017](#)). We calculated models with different parameters like an eccentricity, angular velocities, or inclination angle. We show that these spectra differ from each other and from the spectra of the spherical star. Therefore, the gravitational darkening effect should be included in realistic models of the neutron star atmospheres.

2. MODEL ATMOSPHERES

2.1. *Gravitational darkening*

To calculate model spectra including the gravitational darkening effect, we need to define the geometry of the problem, calculate the effective gravity over the surface of the oblate star, and the intensity spectra at each point on the star. We used the spherical coordinate system where $\theta = 0^\circ$ denotes the latitude of the equator.

In the first approximation, we assume that the shape of the rotating neutron star could be described as an ellipsoid. The radius of this solid is

$$R(\theta) = R_{\text{eq}} \sqrt{1 - e^2 \cos^2(90^\circ - \theta)}, \quad (1)$$

where θ is the latitude in spherical coordinates, R_{eq} is the equatorial radius, whereas R_{p} is the polar radius, and e is eccentricity, defined as $e = \sqrt{(R_{\text{eq}}^2 - R_{\text{p}}^2)/R_{\text{eq}}^2}$.

The effective gravity on the surface of the oblate star depends on the latitude angle. To describe this dependence, we use the approximate formula given by [AlGendy & Morsink \(2014\)](#), Eq. 50 in their work, in the regime of the fast rotation. In the original equation, the colatitude angle was used, whereas in the present paper, we use latitude angle θ , therefore, we replace $\theta' = 90^\circ - \theta$

$$g(\theta)/g_0 = 1 + (c_e \bar{\Omega}^2 + d_e \bar{\Omega}^4 + f_e \bar{\Omega}^6) \sin^2(90^\circ - \theta)$$

$$+ (c_p \bar{\Omega}^2 + d_p \bar{\Omega}^4 + f_p \bar{\Omega}^6 - d_{60} \bar{\Omega}^4) \cos^2(90^\circ - \theta) + d_{60} \bar{\Omega}^4 \cos(90^\circ - \theta), \quad (2)$$

where g_0 is the gravity of a nonrotating star, and the following coefficients with $x = M/R_{\text{eq}}$ are

$$\begin{aligned} c_e &= -0.791 + 0.776x, \\ d_e &= -1.315x + 2.431x^2, \\ f_e &= -1.172x, \\ c_p &= 1.138 - 1.431x, \\ d_p &= 0.653x - 2.864x^2, \\ f_p &= 0.975x, \\ d_{60} &= 13.67x - 27.13x^2. \end{aligned} \quad (3)$$

The dimensionless angular velocity $\bar{\Omega}$ is defined as

$$\bar{\Omega} = \Omega \left(\frac{R_{\text{eq}}^3}{GM} \right)^{1/2}. \quad (4)$$

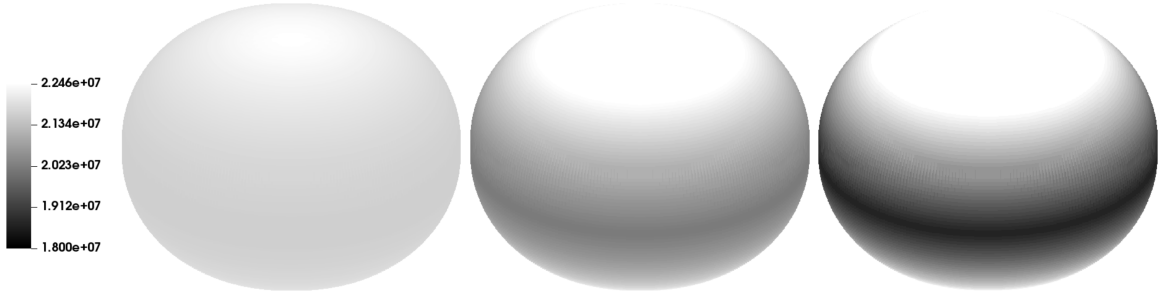


Figure 1. Distribution of the effective temperature over the surface of a neutron star for different dimensionless angular velocities: $\bar{\Omega}^2 = 0.10$ (left panel), $\bar{\Omega}^2 = 0.40$ (middle panel), and $\bar{\Omega}^2 = 0.60$ (right panel). We assumed the effective temperature and surface gravity of an undistorted star: $T_{\text{eff}} = 2.20 \times 10^7$ K and $\log(g) = 14.40$ (cgs), respectively, and Gravitational Darkening Exponent (GDE) $\beta = 0.25$, the eccentricity of the rotating star $e = 0.70$ and inclination angle $i = 30^\circ$.

The local effective gravity and therefore the local effective temperature are strong functions of the dimensionless angular velocity, which we have shown in the example of the distribution of the local temperature in Fig. 1. In the figure, we use the same scale factor for converting values of the temperature into the gray scale. For low values of the $\bar{\Omega}$, the local effective gravity or temperature varies with the latitude angle θ much slowly than for higher values of $\bar{\Omega}$.

Figure 2 shows the dependence of the effective surface gravity on the latitude angle. We assume the gravity of a spherical star $\log(g) = 14.40$ (cgs). As was shown in the

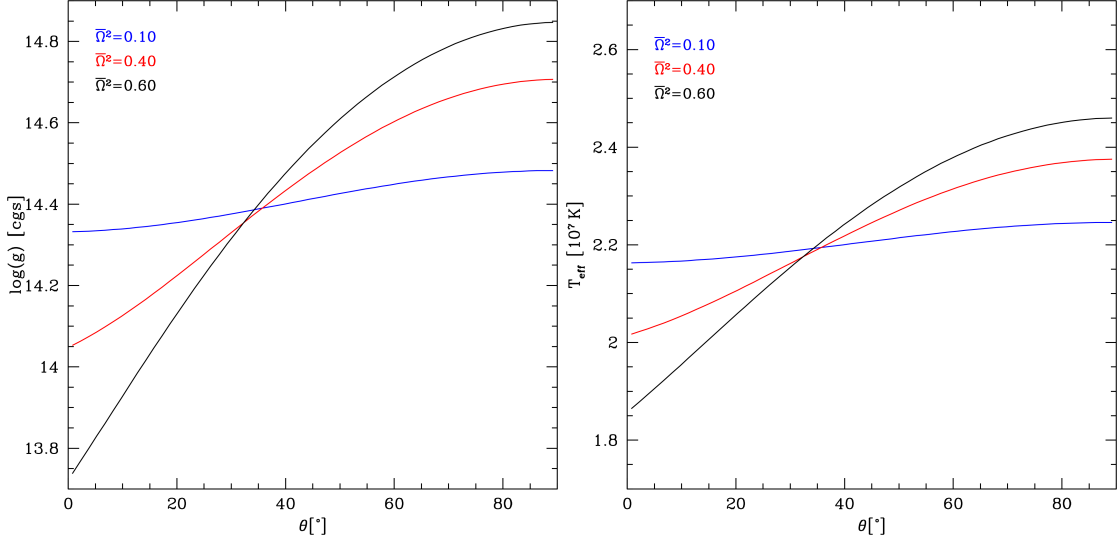


Figure 2. Dependence of the effective gravity (left panel) and the effective temperature (right panel) on the latitude angle θ for various dimensionless angular velocities. We assume the logarithm of the surface gravity of a spherical star $\log(g) = 14.40$ (cgs), the effective temperature of the spherical star $T_{\text{eff}} = 2.20 \times 10^7$ K, GDE $\beta = 0.25$ and various dimensionless angular velocities $\bar{\Omega}^2 = 0.10$ (blue line), 0.40 (red line), and 0.60 (black line).

Fig. 2, the surface gravity on the pole is not equal to the assumed surface gravity of a spherical star $\log(g) = 14.40$. In our calculations, we include the quadrupole moment caused by the mass distribution in the neutron star interior. This moment does not vanish on the pole and causes greater gravity than the gravity of a nonrotating neutron star.

The temperature at a given point on the surface of the neutron star is as follows:

$$T(\theta) = T_{\text{eff}} \left(\frac{g(\theta)}{g_0} \right)^{1/4}, \quad (5)$$

where T_{eff} is the effective temperature of the spherical, nonrotating neutron star, g_0 is the surface gravity of the spherical star, and $g(\theta)$ is the surface gravity at a given point of the distorted star defined by Eq.2.

In the above Eq.5, GDE is equal to 0.25 because we assumed that the atmosphere is radiative. As was shown by (e.g., Lucy 1967), this exponent is different for non-radiative or not fully radiative envelopes. Very recently Claret (2021) calculated self-consistently the GDE for DA and DB white dwarfs. The author showed that this exponent depends not only on the temperature but also on the opacity. In our work we did not calculate GDE. To show how different parameters influence the emergent spectrum, we assume values of the GDE and other parameters. In the Fig. 3, we presented the distribution of the effective temperature over the surface of the oblate star for various GDEs. We assume the dimensionless angular velocity $\bar{\Omega}^2 = 0.60$ and the ratio of the mass to the equatorial radius of the neutron star $x = 0.195$ and $\beta = 0.10, 0.15,$ and 0.25.

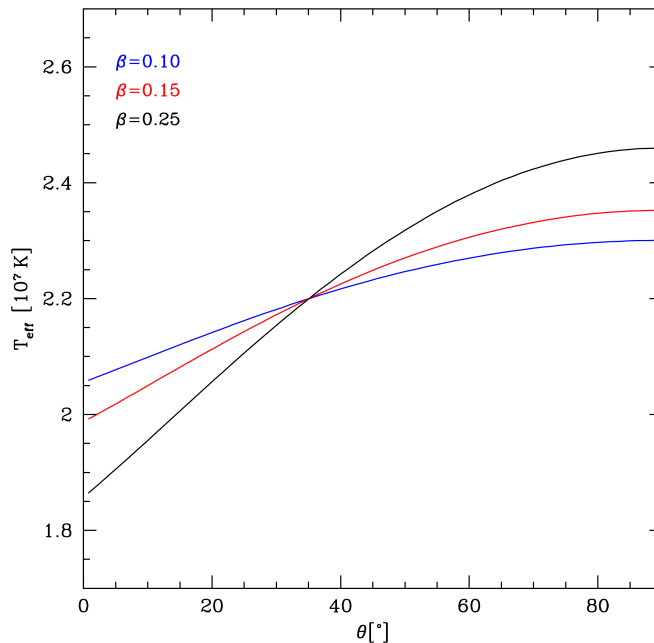


Figure 3. Dependence of the effective temperature on the latitude angle θ for various GDEs: $\beta = 0.25$ denoted by the black line, $\beta = 0.15$ by the red one, and $\beta = 0.10$ by the blue one. We assume the effective temperature of a nonrotating, spherical star, $T_{\text{eff}} = 2.20 \times 10^7 K$, and the logarithm of the surface gravity $\log(g) = 14.40$ (cgs) and dimensionless angular velocity $\bar{\Omega}^2 = 0.60$.

2.2. ATM24

We calculate intensity spectra with the ATM24 code. Our model was described in several papers, e.g., [Madej \(1991\)](#); [Madej et al. \(2004\)](#); [Majczyna et al. \(2005\)](#). The accuracy of our code was recently improved ([Madej et al. 2017](#); [Vincent et al. 2018](#)).

Our code solves the radiative transfer equation in the plane-parallel geometry. In hot atmospheres, Compton scattering plays a crucial role in forming the emerging spectrum and therefore should be treated very carefully. We investigated the scattering of X-ray photons with energies approaching the electron rest mass energy on free, thermal, relativistic electrons. We allow for any large energy exchange between photons and electrons during a single scattering. We assume the equation of state of ideal gas in local thermodynamical equilibrium (LTE). Note that the Compton scattering provides non-LTE effects in the model atmospheres. When calculating opacities, we include energy-dependent free-free and bound-free opacities from all elements with $Z \leq 30$ (atomic number) and bound-bound opacities from hydrogen, helium, and iron.

The equation of transfer was adopted from [Pomraning \(1973, see also Sampson 1959\)](#) and has the following form:

$$\begin{aligned} \mu \frac{dI_\nu}{d\tau_\nu} &= I_\nu - \frac{k_\nu}{k_\nu + \sigma_\nu} B_\nu - \left(1 - \frac{k_\nu}{k_\nu + \sigma_\nu}\right) J_\nu \\ &+ \left(1 - \frac{k_\nu}{k_\nu + \sigma_\nu}\right) J_\nu \int_0^\infty \Phi(\nu, \nu') \left(1 + \frac{c^2}{2h\nu'^3} J_{\nu'}\right) d\nu' + \end{aligned}$$

$$\begin{aligned}
& -\frac{k_\nu}{k_\nu + \sigma_\nu} \left(1 + \frac{c^2}{2h\nu^3} J_\nu \right) \\
& \times \int_0^\infty \Phi(\nu, \nu') J_{\nu'} \left(\frac{\nu}{\nu'} \right)^3 \exp \left[-\frac{h(\nu - \nu')}{kT} \right] d\nu',
\end{aligned} \tag{6}$$

where k_ν and σ_ν denote coefficients of absorption and electron scattering, respectively. I_ν is the energy-dependent specific intensity, J_ν is the mean intensity of radiation, and z is the geometrical depth in the atmosphere. We formulated the exact angle-averaged redistribution function $\Phi(\nu, \nu')$ and the Compton scattering cross section $\sigma(\nu \rightarrow \nu', \vec{n} \cdot \vec{n}')$ (for details, see [Madej et al. \(2017\)](#); [Nagirner & Poutanen \(1993, 1994\)](#)). The equation of transfer is solved together with the hydrostatic and radiative equilibrium equations because we assume that the atmosphere is static and that only photons transport the energy accumulated in the core of the neutron star. We neglect the influence of the magnetic field, accretion, and the effect of electron degeneracy, which is unimportant in the hot atmospheres. The limb-darkening/-brightening effects are fully taken into account in our computations.

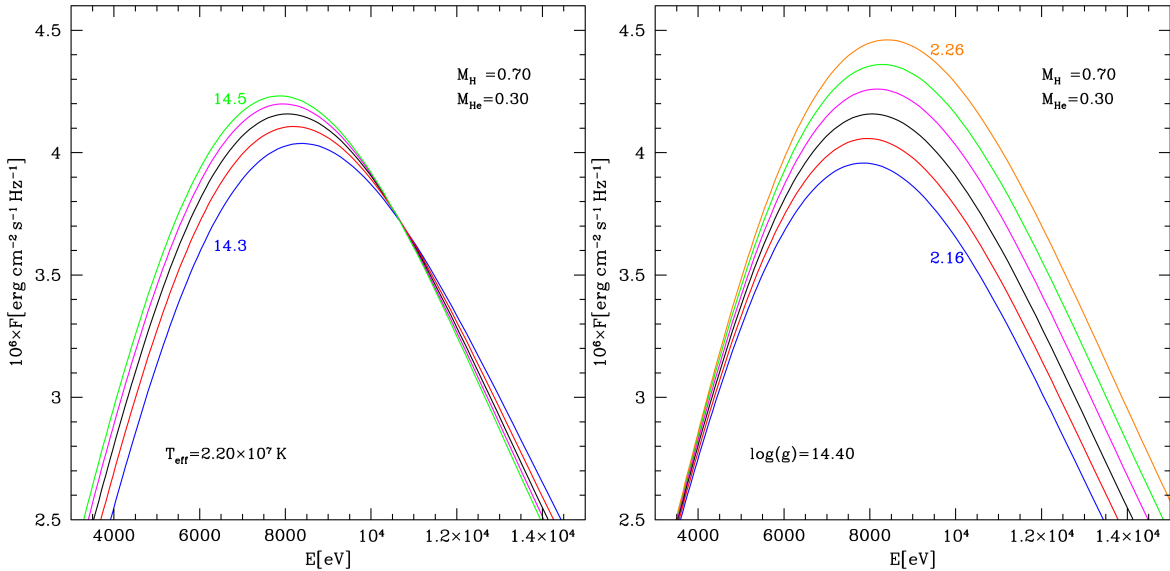


Figure 4. Theoretical spectra of the unit surface calculated by the ATM24 code for different values of the effective temperatures and surface gravities. In the left panel, we show the theoretical spectra for the effective temperatures $T_{\text{eff}} = 2.20 \times 10^7$ K and various surface gravities from $\log(g) = 14.30$ (cgs) to $\log(g) = 14.50$ (cgs). In the right panel we show spectra for the fixed surface gravity $\log(g) = 14.40$ (cgs) and various effective temperatures from $T_{\text{eff}} = 2.16 \times 10^7$ K to $T_{\text{eff}} = 2.26 \times 10^7$ K.

We assumed that the rotating neutron star is seen at some inclination to the equatorial plane. Input parameters of the ATM24 code are the effective temperature, surface gravity, and the chemical composition. We assumed that the reference nonrotating star has the effective temperature $T_{\text{eff}} = 2.20 \times 10^7$ K and the surface gravity $\log(g) = 14.40$ (cgs). The atmosphere consists of hydrogen and helium with the cosmic mass abundance $M_{\text{H}} = 0.70$ and $M_{\text{He}} = 0.30$.

In X-ray bursters, especially during the burst and soon after, we expect high temperatures of the gas, so $T_{\text{eff}} = 2.20 \times 10^7$ K is a reasonable assumption. Values of the effective temperature and the logarithm of the surface gravity of the spherical star were taken arbitrarily. The chemical composition of X-ray burst sources is very poorly constrained. It is frequently assumed that the atmosphere consists of hydrogen and helium in arbitrarily chosen proportions. For example, [Galloway et al. \(2006\)](#) investigated Eddington-limited bursts from 4U 1636-536. For this source, a hydrogen-rich atmosphere with $M_{\text{H}} = 0.70$ as well as a pure helium atmosphere were investigated. Therefore, we assume chemical composition with cosmic hydrogen abundance.

The rotating star is oblate, therefore the gravity and the effective temperature are different at various latitude angles. We calculated the local effective gravity and the local effective temperature according to the formulae given by Equations 2 and 5. These local values of the gravity and the effective temperature are input parameters for the calculation of monochromatic specific intensities at various latitude angles. These intensities were next integrated over the whole surface to obtain the spectrum as seen by a distant observer.

For a given eccentricity of the distorted star, we were able to compute the distance from the center of gravity for each patch on the surface and its area (in cm^2), its latitude, and the azimuth as seen by the observer. Simultaneously, we determined the cosine of the projection angle as seen by the observer. We determined the effective gravity as a function of the latitude. Therefore, we know all variables that are necessary to integrate the emergent intensity over various patches to obtain the final monochromatic luminosity of the distorted star.

In our ATM24 code, we include the limb-darkening effect and now we add the gravitational darkening effect. An example of flux spectra of the spherical star calculated by the ATM24 code is presented in Figure 4. In the left panel, we compare the spectra for the same chemical compositions given above and the same effective temperatures but different surface gravities from $\log(g) = 14.30$ up to 14.50 (cgs). With increasing surface gravity, spectra become softer, and their maximum shifts toward lower energies. The right panel shows our model spectra calculated for the same surface gravity and different effective temperatures from $T_{\text{eff}} = 2.16 \times 10^7$ up to 2.24×10^7 K. With increasing temperature, the maximum of the spectra shifts toward higher energies.

3. SPECTRA OF THE ROTATING NEUTRON STAR

We computed a small grid of theoretical spectra of the rotating neutron stars (56 model spectra). Because the calculations are very time consuming, we divided the star into 18×36 points in latitude and azimuthal angles. As was mentioned above, we assumed parameters of the rotating star like the effective temperature of the spherical star $T_{\text{eff}} = 2.20 \times 10^7$ K, surface gravity of the nonrotating star $\log(g) = 14.40$ (cgs), chemical composition ($M_{\text{H}} = 0.70$ and $M_{\text{He}} = 0.30$) and mass to radius ratio $x = 0.195$. We computed our theoretical spectra for different values of the

other parameters: the dimensionless angular velocity $\bar{\Omega}^2 = 0.30$ and 0.60 , and few inclination angles from $i = 0^\circ$ up to 90° with step $\Delta i = 10^\circ$. We note that the both assumed values of the dimensionless angular velocity are relevant for the fast-rotation limit.

The eccentricity of the rotating neutron star depends on the angular velocity of the rotation. The formula that connects these two variables depends on the equation of state of the matter building up neutron star. Such approximate formulae were proposed by various authors (see e.g., [AlGendy & Morsink 2014](#); [Silva et al. 2021](#)). In our paper, we used the relation from [Silva et al. \(2021\)](#).

$$e = 0.251 + 0.935\bar{\Omega}^2 + 0.709x + 0.030\bar{\Omega}^2x - 0.472\bar{\Omega}^4 - 2.427x^2 \quad (7)$$

Here, we quoted Eq.19 from [Silva et al. \(2021\)](#) using variables defined in our paper. For the assumed $x = 0.195$ and $\bar{\Omega}^2 = 0.30$ and 0.60 , the eccentricity of the flattened star is equal to $e = 0.54$ and 0.69 , respectively. These values of the eccentricity were used during the calculations of theoretical spectra of rotating neutron star. In some cases where we show the influence of the shape of the star on the emergent spectrum, we thread the eccentricity as a free parameter, independent of the angular velocity (see Fig. 5).

Assuming $\bar{\Omega}^2 = 0.30$, and 0.60 , $x = 0.195$ and two representative equations of state ([AlGendy & Morsink 2014](#)) calculated the frequency of the neutron star rotation (see Tables 2 and 3 in their paper). For both dimensionless angular velocities they obtained high frequencies, e.g., for $\bar{\Omega}^2 = 0.30$, $M = 1.80 M_\odot$ and $R = 13.6$ km (EOS HLPS2) the frequency is equal to $\nu = 842$ Hz whereas for $\bar{\Omega}^2 = 0.60$, $M = 1.99 M_\odot$ and $R = 15.1$ km (EOS HLPS2), $\nu = 1084$ Hz. The highest measured frequency of the rotation is equal to 716 Hz in the case of pulsar PSR J1748-2446ad ([Hessels et al. 2006](#)). For X-ray bursters, the fastest spin of the neutron star equals to $\nu = 620$ Hz for 4U 1608-522 ([Muno et al. 2002](#)). The maximal value of the frequency of the neutron star rotation depends on the equation of state, and it is as high as 1200 Hz (see e.g., [Haensel et al. 2007](#)).

Figure 5 (top panel) shows theoretical spectra of the rotating star with different eccentricities for the same inclination angle $i = 30^\circ$. We note that these spectra have very similar shapes. It may appear that these spectra differ only in the normalization. For this reason, in the lower panel of the Figure 5 we show the ratio of the monochromatic flux emitted by the star with $e = 0.30$ and the flux of the star with $e = 0.69$. If these spectra differ only by the normalization, this ratio should be constant across the whole range of photon energies, which is not the case presented in the figure. Of course, for lower differences of the eccentricity, the ratio is closer to constant so the spectra have more similar shapes. It is especially important for methods of mass and radius determination that used the distance to the source (see e.g., the review by [Bhattacharyya 2010](#)). Our mass and radius determination method

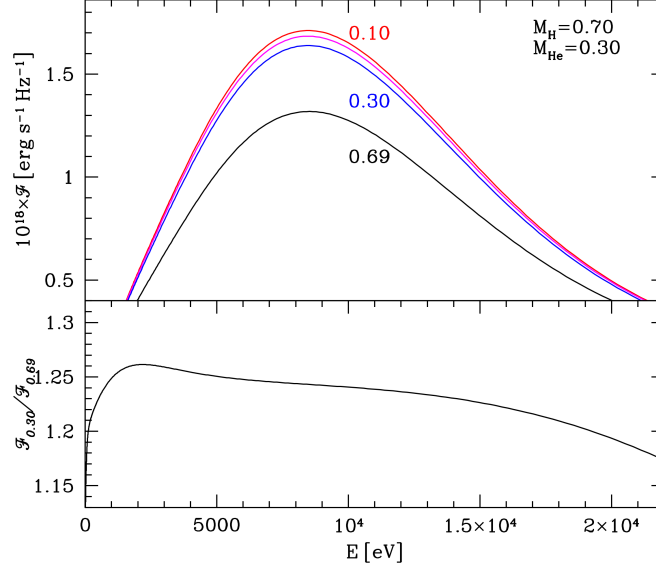


Figure 5. The top panel shows the theoretical spectra of the flattened neutron star for a given parameters: $T_{\text{eff}} = 2.20 \times 10^7$ K, $\log(g) = 14.40$ (cgs), $i = 30^\circ$, $\bar{\Omega}^2 = 0.60$ and different values of the eccentricity of the star $e = 0.10$ (red line), 0.20 (magenta), 0.30 (blue), and 0.69 (black). The lower panel shows the ratio of the monochromatic flux ($\mathcal{F}_{0.30}$) emitted by the ellipsoidal star with $e = 0.30$ and flux ($\mathcal{F}_{0.69}$) emitted by a star with $e = 0.69$.

(e.g., [Majczyna & Madej 2005](#)) is independent of the distance; therefore value of the obtained normalization does not affect our results.

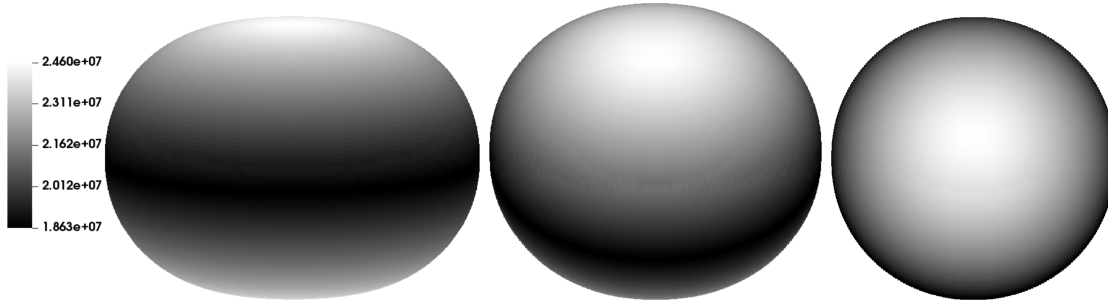


Figure 6. Distribution of the local effective temperature over the surface of the neutron star seen by a distant observer. We assume parameters of our reference model for T_{eff} and $\log(g)$ and the gravitational darkening exponent $\beta = 0.25$, dimensionless angular velocity $\bar{\Omega}^2 = 0.60$ and different inclination angles $i = 10^\circ$ (left panel), $i = 40^\circ$ (middle panel), and $i = 80^\circ$ (right panel).

Figure 6 shows the temperature distribution on the star seen at different inclination angles $i = 30^\circ$ (left panel), $i = 60^\circ$ (middle), and $i = 80^\circ$ (right panel). The last panel of this figure presents the star seen almost at the pole on, where the temperature has the highest value.

The spectral shape significantly depends on the inclination angle as was shown in the Figure 7. An inclination angle equal to $i = 90^\circ$ denotes that an observer sees the star at the pole, whereas $i = 0^\circ$ is in the equatorial plane. As the inclination angle

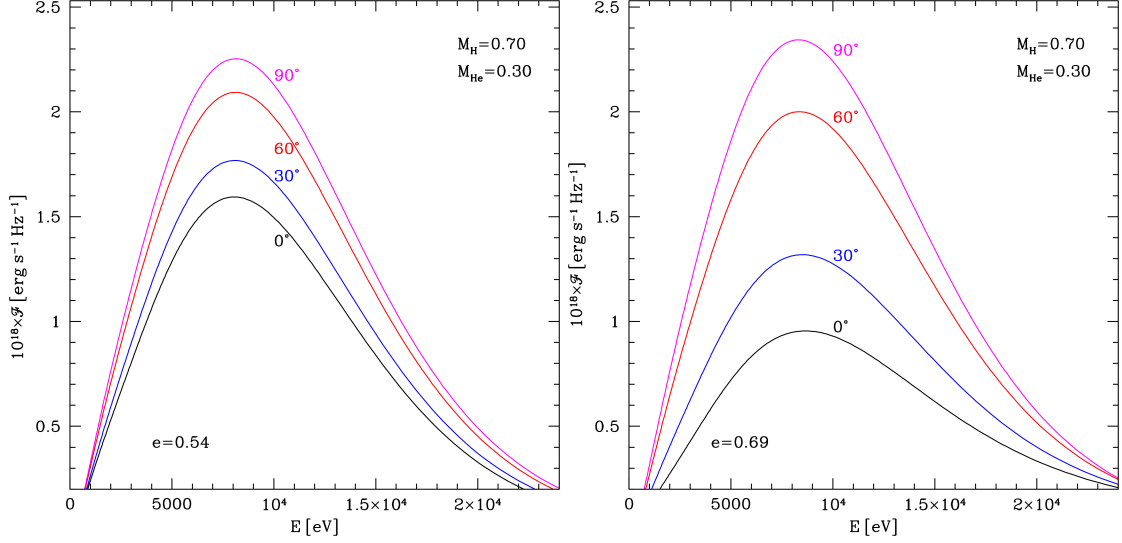


Figure 7. Theoretical spectra of the rotating neutron star for various inclination angles. We assumed parameters $T_{\text{eff}} = 2.20 \times 10^7$ K, $\log(g) = 14.40$ (cgs), $\beta = 0.25$, and two values of the dimensionless angular velocity $\bar{\Omega}^2 = 0.30$ (left panel) and $\bar{\Omega}^2 = 0.60$ (right panel).

increases the observer sees hotter and hotter areas, but the spectrum does not become harder and its maximum shifts toward lower energies. This slightly unintuitive effect is connected with the different contributions of spots with different temperatures when the inclination angle changes. Hotter areas located at the poles are smaller than those colder ones located at the equatorial plane.

Figure 8 shows spectra emitted by the rotating star calculated for various effective temperatures of the spherical star. The left panel shows spectra of the neutron star rotating with $\bar{\Omega}^2 = 0.30$, whereas the right one is rotating with $\bar{\Omega}^2 = 0.60$. In both cases, we assume the logarithm of gravity of the nonrotating star $\log(g) = 14.40$ (cgs). The dashed line denotes spectra of the spherical star. This star has various values of temperature ($T_{\text{eff}} = 1.0 \times 10^7$ K, 1.6×10^7 K and 2.2×10^7 K respectively) constant over the surface. The maxima of spectra with gravitational darkening effect are shifted toward higher energies, and spectra are harder than these emitted by the spherical star.

Table 1 presents examples of a few values of the effective and color temperatures for models with two values of the dimensionless angular velocities $\bar{\Omega}^2 = 0.30$ and 0.60 and a few inclination angles i . As to be expected, stars seen in the equatorial plane ($i = 0^\circ$) have the lowest effective temperatures ($T_{\text{eff}} = 2.117 \times 10^7$ K and $T_{\text{eff}} = 2.001 \times 10^7$ K for $\bar{\Omega}^2 = 0.30$ and 0.60 , respectively), the lowest color temperatures, and the lowest bolometric fluxes. On the contrary, stars seen pole on are brighter and apparently hotter. The last column of the Table 1 contains spectral hardening factor $f_c = T_c/T_{\text{eff}}$ (here, T_c is the color temperature whereas T_{eff} is the effective temperature). The color temperature is calculated from the Wien displacement law $h\nu_{\text{max}} = 2.82kT$. The value of the hardening factor depends on the inclination angle as well as on the

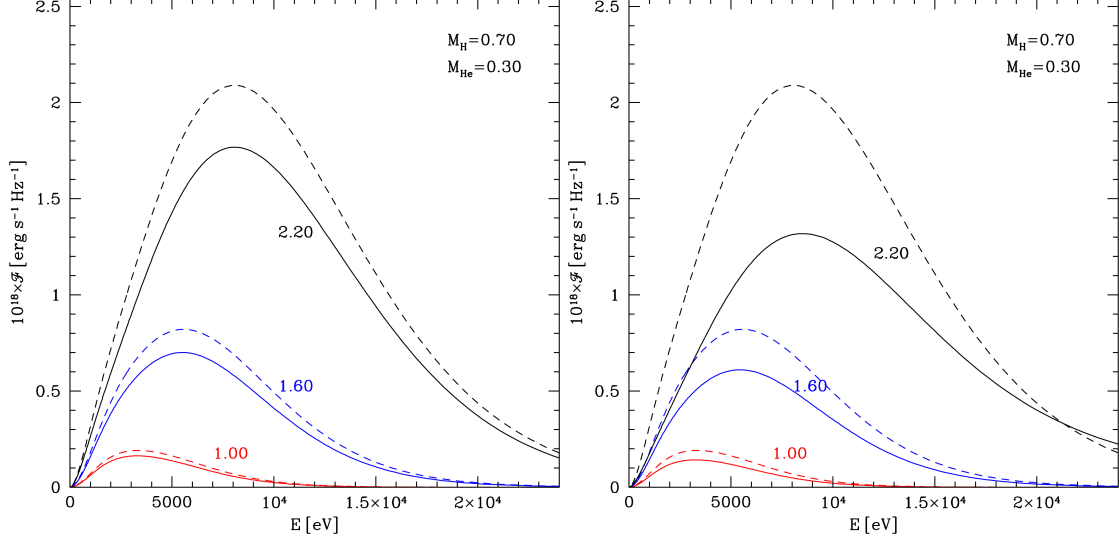


Figure 8. Theoretical spectra of the rotating star for different effective temperatures of the spherical neutron star. We fixed following the parameters: $\log(g) = 14.40$, $\beta = 0.25$, $i = 30^\circ$, and $\bar{\Omega}^2 = 0.30$; $e = 0.54$ (left panel) and $\bar{\Omega}^2 = 0.60$; $e = 0.69$ (right panel). The black solid curve denotes spectrum of the oblate star calculated for assumed temperatures of the spherical star $T_{\text{eff}} = 2.20 \times 10^7$ K whereas blue ones assume $T_{\text{eff}} = 1.60 \times 10^7$ K and red $T_{\text{eff}} = 1.00 \times 10^7$ K. Black, blue, and red dashed curves denote spectra of the spherical stars with appropriate temperatures.

Table 1. Bolometric luminosities and effective temperatures of the rotating, flattened neutron star with two dimensionless angular velocities $\bar{\Omega}^2$ and a few inclination angles i . We assumed the effective temperature of the spherical star $T_{\text{sph}} = 2.20 \times 10^7$ K. The bolometric luminosity of the spherical star is equal to $L_{\text{sph}} = 8.179 \times 10^{37}$ erg s $^{-1}$ and color temperature $T_c = 3.31 \times 10^7$ K. We assume that the equatorial radius of the oblate star and the radius of the spherical star is equal to $R = 7$ km.

$\bar{\Omega}^2 = 0.30$ ($e = 0.54$)						
Model	$L_{\text{bol}} \times 10^{37}$	$L_{\text{bol}}/L_{\text{sph}}$	$T_{\text{eff}} \times 10^7$ K	$T_{\text{eff}}/T_{\text{sph}}$	$T_c \times 10^7$ K	f_c
$i = 0.0$	6.365	0.78	2.1165	0.962	3.31199	1.565
$i = 30$	7.103	0.87	2.1753	0.989	3.31199	1.523
$i = 90$	9.159	1.12	2.3181	1.054	3.36002	1.449
$\bar{\Omega}^2 = 0.60$ ($e = 0.69$)						
Model	$L_{\text{bol}} \times 10^{37}$	$L_{\text{bol}}/L_{\text{sph}}$	$T_{\text{eff}} \times 10^7$ K	$T_{\text{eff}}/T_{\text{sph}}$	$T_c \times 10^7$ K	f_c
$i = 0.0$	4.805	0.59	2.0007	0.909	3.55911	1.779
$i = 30$	6.164	0.75	2.1292	0.968	3.50826	1.648
$i = 90$	9.827	1.20	2.3926	1.088	3.40870	1.425

dimensionless angular velocity. The largest values of f_c were obtained for the star seen pole on whereas the lowest ones were for the star seen in the equatorial plane. For the spherical star with reference parameters $T_{\text{eff}} = 2.20 \times 10^7$ K and $\log(g) = 14.40$ (cgs),

the spectral hardening factor is equal to $f_c = 1.50$ and differs from values for the flattened star given in the last column of the table.

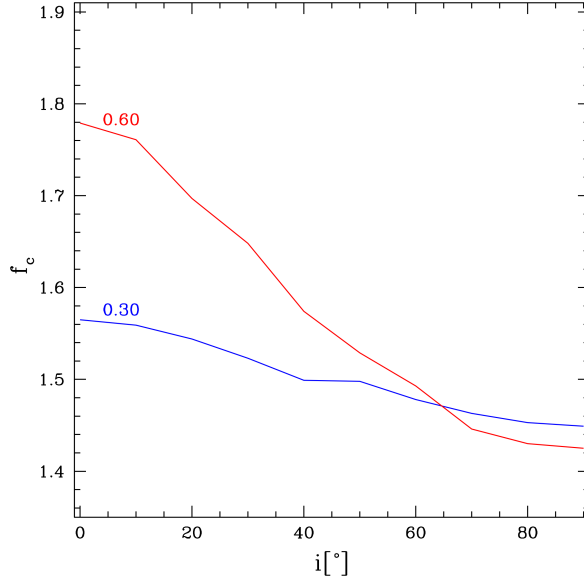


Figure 9. Spectral hardening factor f_c for a flattened star with our reference parameters seen at different inclination angles i and two sets of parameters $\bar{\Omega}^2 = 0.30$ and $e = 0.54$ (blue line labeled 0.30) and $\bar{\Omega}^2 = 0.60$ and $e = 0.69$ (red line labeled 0.60).

Figure 9 presents the dependence of the spectral hardening factor for a rotationally flattened neutron star with two values of the dimensionless angular velocity $\bar{\Omega}^2 = 0.30$ and 0.60 on inclination angles from $i = 0^\circ$ (star seen in the equatorial plane) up to $i = 90^\circ$ (seen pole on). For stars with higher values of the angular velocity of the rotation and therefore an eccentricity, the spectral hardening factor has larger values and changes more rapidly with the inclination angle than in the case of the stars with a lower value of $\bar{\Omega}^2$.

4. SUMMARY AND DISCUSSION

In our paper, we presented spectra of a rotationally distorted neutron star considering also the case of fast rotation. We have shown the substantial influence of both the dimensionless angular velocity $\bar{\Omega}^2$ and the inclination angle i on the emitted spectra.

Using the ATM24 code we calculated a small sample grid of theoretical spectra integrated over the distorted surface of a sample rotating neutron star seen by a distant observer at various inclination angles. We assumed the following parameters: two dimensionless angular velocities $\bar{\Omega}^2 = 0.30$ and 0.60 , the effective temperature of the nonrotating star $T_{\text{eff}} = 2.20 \times 10^7$ K, the logarithm of the surface gravity of the spherical star $\log(g) = 14.40$ (cgs) and inclination angles from $i = 0^\circ$ to $i = 90^\circ$ with the step $\Delta i = 10^\circ$. We assume that the atmosphere is a mixture of hydrogen and helium with $M_{\text{H}} = 0.70$ and $M_{\text{He}} = 0.30$.

The effective gravity and the effective temperature (determined from von Zeipel law) are strong functions of the dimensionless angular velocity $\bar{\Omega}^2$ (see Eq.2). Therefore, $\bar{\Omega}^2$ belongs to parameters that play a crucial role in the formation of the emergent spectrum. The eccentricity of the oblate star depends on $\bar{\Omega}^2$ and was obtained by the approximate (independent of the equation of state) formula from [Silva et al. \(2021\)](#).

[Suleimanov et al. \(2020\)](#) have shown the spectra of the rotating neutron star as a function of the inclination angle and the angular velocity of the star. They applied a diluted blackbody spectrum to describe the local emission corrected by the hardening factor. The authors assumed slow-rotation approximation during the calculation of the effective gravity. Their Constant Relative Flux model is the same as our model of a flattened neutron star with the effective temperature proportional to the local effective gravity as $T_{\text{eff}}(\theta) \sim g(\theta)^{0.25}$. Therefore, our model corresponds to the upper panel of the Figure 6 in their paper. The lower panel of Fig.6 in their paper simply ignores the von Zeipel law. The paper mentioned above was based on the code defined in [Suleimanov et al. \(2012\)](#), where the equation of transfer has part of the stimulated Compton scattering terms artificially transferred to the denominator (see Eq. 12 their paper). As a result expression for the source function was depleted by one of the Compton-induced scattering terms (see Eq. 14). The impact of such an arbitrary change in their paper on the atmosphere models near the Eddington limit is unknown. In the ATM 24 code, such an artificial manipulation does not exist.

In our model we applied fast rotation approximation; therefore, we included the quadrupole moment of the mass distribution in the neutron star interior. We calculated very carefully specific intensities $I_\nu(T_{\text{eff}}(\theta), g_{\text{eff}}(\theta))$ at each patch on the surface. These specific intensities are next integrated over the surface of the neutron star to obtain spectra that could be seen by the distant observer ([Róžańska et al. 2017, 2018](#)). Spectra presented in this paper are not corrected for the relativistic effects, which will be the subject of our future work. In our paper, we did not include effects of the special relativity (relativistic Doppler broadening), which change the shape of the spectrum. This has been investigated by [Bauböck et al. \(2015\)](#) for a perfect black body spectrum. Authors concluded that changes due to Doppler broadening are small compared to the gravitational redshift.

In this paper, we clearly showed that the gravitational darkening effect should be included in realistic calculations of the rotating neutron star spectra. This effect modifies the shape of the emerging spectrum and therefore affects the determination of neutron star parameters obtained by spectral fitting of real data.

This work was supported by grant No. 2015/17/B/ST9/03422 from the Polish National Science Center.

REFERENCES

- AlGendy, M. & Morsink, S. M. 2014, *ApJ*, 791, 78
- Bauböck, M., Özel, F., Psaltis, D., & Morsink, S. M. 2015, *ApJ*, 799, 22

- Belvedere, R., Boshkayev, K., Rueda, J. A., & Ruffini, R. 2014, *Nuclear Physics A*, 921, 33
- Bhattacharyya, S. 2010, *AdSpR*, 45, 949
- Claret, A. 2015, *A&A*, 577, A87
- Claret, A. 2021, *A&A*, 648, A111
- Djurašević, G., Rovithis-Livaniou, H., Rovithis, P., et al. 2003, *A&A*, 402, 667
- Djurašević, G., Rovithis-Livaniou, H., Rovithis, P., et al. 2006, *A&A*, 445, 291
- Domiciano de Souza, A., Kervella, P., Moser Faes, D., et al. 2014, *A&A*, 569, A10
- Galloway, D. K., Muno, M. P., Hartman, J. M., Psaltis, D., & Chakrabarty, D. 2008, *ApJS*, 179, 360
- Galloway, D. K., Psaltis, D., Muno, M. P., & Chakrabarty, D. 2006, *ApJ*, 639, 1033
- Haensel, P., Potekhin, A. Y., & Yakovlev, D. G. 2007, *Neutron Stars I. Equation of State and Structure*, Springer
- Hessels, J. W. T., Ransom, S. M., Stairs, I. H., et al. 2006, *Science*, 311, 1901
- Jaroszynski, M. 1986, *AcA*, 36, 355
- Lucy, L. B. 1967, *Zeitschrift für Astrophysik*, 65, 89
- Madej, J. 1991, *ApJ*, 376, 161
- Madej, J., Joss, P. C., & Różańska, A. 2004, *ApJ*, 602, 904
- Madej, J., Różańska, A., Majczyna, A., & Należyty, M. 2017, *MNRAS*, 469, 2032
- Majczyna, A. & Madej, J. 2005, *AcA*, 55, 349
- Majczyna, A., Madej, J., Joss, P. C., & Różańska, A. 2005, *A&A*, 430, 643
- Muno, M. P., Chakrabarty, D., Galloway, D. K., & Psaltis, D. 2002, *ApJ*, 580, 1048
- Nagirner, D. I. & Poutanen, Y. J. 1993, *Astronomy Letters*, 19, 262
- Nagirner, D. I. & Poutanen, Y. J. 1994, *Astrophysics and Space Physics Reviews*, 9, 1
- Pomraning, G. C. 1973, *The equations of radiation hydrodynamics*
- Różańska, A., Beldycki, B., Madej, J., Adhikari, T. P., & You, B. 2017, *AcA*, 67, 51
- Różańska, A., Bresler, K., Beldycki, B., Madej, J., & Adhikari, T. P. 2018, *A&A*, 612, L12
- Sampson, D. H. 1959, *ApJ*, 129, 734
- Silva, H. O., Pappas, G., Yunes, N., & Yagi, K. 2021, *PhRvD*, 103, 063038
- Suleimanov, V., Poutanen, J., & Werner, K. 2012, *A&A*, 545, 120
- Suleimanov, V. F., Poutanen, J., & Werner, K. 2020, *A&A*, 639, A33
- Vincent, F. H., Bejger, M., Różańska, A., et al. 2018, *ApJ*, 855, 116
- von Zeipel, H. 1924, *MNRAS*, 84, 665
- Webbink, R. F. 1976, *ApJ*, 209, 829